Chemical Geology 614 (2022) 121177

Contents lists available at ScienceDirect

Chemical Geology

journal homepage: www.elsevier.com/locate/chemgeo

Production of Cr(VI) from $Cr_xFe_{1-x}(OH)_3$ precipitates and NOM-Cr(III) colloids upon reaction with H_2O_2 under oxic conditions

Binrui Li [a,1], Shaojian Zhang [b,1], Peng Liao [b,*], Peng Liu [c], Zhihang Ye [c], Chongxuan Liu [a,*]

[a] State Environmental Protection Key Laboratory of Integrated Surface Water-Groundwater Pollution Control, School of Environmental Science and Engineering, Southern University of Science and Technology, Shenzhen 518055, PR China
[b] State Key Laboratory of Environmental Geochemistry, Institute of Geochemistry, Chinese Academy of Sciences, Guiyang 550081, PR China
[c] School of Environment, China University of Geosciences, 388 Lumo Road, Wuhan 430074, PR China

ARTICLE INFO

Editor: Dr. Hailiang Dong

Keywords:
$Cr_xFe_{1-x}(OH)_3$ precipitates
NOM-Cr(III) colloids
Hydrogen peroxide
Cr(III) oxidation
Cr(VI) generation

ABSTRACT

Cr(III)-Fe(III) hydroxides ($Cr_xFe_{1-x}(OH)_3$ precipitates) and NOM-Cr(III) colloids are common products of Cr(VI) reduction during remediation and natural processes. However, re-oxidation of Cr(III) to Cr(VI) can undermine remediation efforts. Nevertheless, until now, less is known about the oxidation of Cr(III) from naturally occurring Cr(III) (i.e., $Cr_xFe_{1-x}(OH)_3$ precipitates and NOM-Cr(III) colloids) by H_2O_2. Here, we examined the oxidation of Cr(III) from $Cr_{0.5}Fe_{0.5}(OH)_3$ and NOM-Cr(III) colloids by H_2O_2 under oxic conditions. Batch experiments demonstrated that Cr(VI) generation via Cr(III) oxidation from both $Cr_{0.5}Fe_{0.5}(OH)_3$ and NOM-Cr(III) colloids increased with increasing H_2O_2 concentration. Increasing pH and addition of Fe^{2+} promoted Cr(III) oxidation, but the promoting effect of pH was more significant on $Cr_{0.5}Fe_{0.5}(OH)_3$, whereas the promoting effect of Fe^{2+} was significant on NOM-Cr(III) colloids. By evaluating the effects of Fe species on Cr(VI) generation from $Cr_{0.5}Fe_{0.5}(OH)_3$ and NOM-Cr(III) colloids, we proposed that an intermediate reactive Fe species formed during the reaction with H_2O_2 activated Cr(III) oxidation. X-ray photoelectron spectroscopy (XPS) and X-ray absorption fine structure (XAFS) analyses collectively supported that the surface structural Fe in $Cr_xFe_{1-x}(OH)_3$ precipitates might contribute to the formation of reactive Fe species that promoted Cr(III) oxidation. In contrast, the decomposition of complexed NOM from NOM-Cr(III) colloids enabled the formation of Cr(III)-H_2O_2 complex that is favorable for subsequent Cr(III) oxidation. Results gained from this study provide a complete understanding of the long-term stability of naturally occurring Cr(III) under environmentally relevant conditions.

1. Introduction

Chromium (Cr) is a priority contaminant in soils and groundwater as a result of industrial activities and natural processes. Toxic Cr(VI) ($HCrO_4^-$ and CrO_4^{2-}) is highly soluble and poses a serious threat to humans and ecosystems (Palmer and Wittbrodt, 1991; Wielinga et al., 2001). In contrast, the reduced form of trivalent Cr (Cr(III)) is relatively immobile and less toxic (Barnhart, 2008), which had a limited solubility (6×10^{-31}, 298 K) under slightly acidic to slightly alkaline pH conditions (Palmer and Wittbrodt, 1991; Rai et al., 2002; Rai et al., 1987). Therefore, reduction of Cr(VI) to Cr(III) is the most common remediation strategy to mitigate Cr(VI) contamination. In subsurface environments, the reduced Cr(III) is closely associated with Fe forming Cr(III)-Fe(III) hydroxides ($Cr_xFe_{1-x}(OH)_3$) owing to the wide application of iron-based materials such as Fe(II)-containing minerals and zerovalent iron in engineering remediation sites (Bishop et al., 2014; Chang et al., 2014; Hu et al., 2004; Loyaux-Lawniczak et al., 2000; Williams and Scherer, 2001) and ubiquity of iron minerals in nature (Singh et al., 2002; Trolard et al., 1995). Compared to pure $Cr(OH)_3$, $Cr_xFe_{1-x}(OH)_3$ precipitates have a much lower Cr(III) solubility (Pan et al., 2017; Sass and Rai, 1987). For example, the solubility of Cr(III) from $Cr_xFe_{1-x}(OH)_3$ is several orders of magnitude lower than that from $Cr(OH)_3$ at the same pH (Pan et al., 2017). In addition to Fe, natural organic matter (NOM) can also reduce Cr(VI) to Cr(III), resulting in the formation of NOM-Cr (III) complexes (Fan et al., 2019; Gustafsson et al., 2014; Li et al., 2020; Zhang et al., 2022a). In contrast to $Cr_xFe_{1-x}(OH)_3$ precipitates, NOM-Cr(III) complexes typically exist in the form of colloids with particle size ranging from ca. 3 nm to 450 nm, allowing the high mobility of

* Corresponding authors.
E-mail addresses: liaopeng@mail.gyig.ac.cn (P. Liao), liucx@sustech.edu.cn (C. Liu).
[1] These authors contributed equally.

https://doi.org/10.1016/j.chemgeo.2022.121177
Received 28 August 2022; Received in revised form 12 October 2022; Accepted 13 October 2022
Available online 17 October 2022
0009-2541/© 2022 Elsevier B.V. All rights reserved.

Cr(III) (Landrot et al., 2012; Li et al., 2022). Such propensities underline that the co-existence of Fe or NOM with Cr(III) could alter the geochemical reactivity of Cr(III) from $Cr_xFe_{1-x}(OH)_3$ precipitates and NOM-Cr(III) colloids, modulating the long-term stabilization of reduced Cr(III) in contaminated sites.

Redox conditions shift from reducing to oxidizing conditions due to natural processes (e.g., flooding, surface water intrusion, and seasonal water table fluctuations) and anthropogenic events (e.g., dredging and groundwater recharge) can cause the reoxidation of Cr(III) to Cr(VI) (Boman et al., 2008; Diem et al., 2013; Peiffer et al., 2021; Ramesh Kumar and Riyazuddin, 2012). In natural environments, oxidation of Cr (III) to Cr(VI) by oxygen is slow with rate on the order of days to years under neutral pH conditions (Schroeder and Lee, 1975), but the oxidation by Mn-containing minerals is fast on orders of minutes to hours (Bartlett and James, 1979; Fandeur et al., 2009; Ivarsson et al., 2011; Landrot et al., 2012; Liu et al., 2020; Liu et al., 2021; Oze et al., 2007; Pan et al., 2017). Thus, oxidation of Cr(III) by Mn oxides have long been regarded as the principal pathway for Cr(III) oxidation. On the other hand, in engineered sites such as the drinking water distribution systems, due to the wide and long-term application of Cr in plumbing materials, Cr(III) can accumulate to high levels (Cui et al., 2016; Frey et al., 2005; Liu et al., 2016) and react with residual disinfectant chlorine to result in the risk of Cr(VI) generation at the tap (Chebeir and Liu, 2018; Lai and McNeill, 2006; Lindsay et al., 2012; McNeill et al., 2012).

Besides Mn minerals and chlorine, hydrogen peroxide (H_2O_2) is also a potent oxidant that can oxidize Cr(III) (hydr)oxides. H_2O_2 can be widely produced in biological, weathering, and photochemical processes in terrestrial environments (Foustoukos et al., 2011; Oze et al., 2016). For example, the detected H_2O_2 concentration ranges from 1 to 100 μM in rainwater (Qin et al., 2017a; Qin et al., 2017b) and from 3.5 to 7.0 μM in groundwater (Cooper and Zika, 1983; Moffett and Zika, 1987). A much higher H_2O_2 concentration, up to 10 M, can occur in contaminated sites for subsurface remediation (Yang et al., 2019), because H_2O_2 is frequently used for in situ chemical oxidation (ISCO) of contaminated soil and groundwater due to its high oxidizing capability towards organic contaminants (Pardieck et al., 1992; Yang et al., 2019). Oxidation of Cr(III) to Cr(VI) by H_2O_2 has been frequently observed (Eq. 1) (Oze et al., 2007; Oze et al., 2016; Rao et al., 2002; Rock et al., 2001), which is pH-dependent (Bokare and Choi, 2011; Rao et al., 2002) and proceeds via forming Cr(III)-peroxide complexes first (Knoblowitz and Morrow, 1976). At acidic pH, Cr(III) ion exists as hexaaquo ion $[Cr(H_2O)_6]^{3+}$ ($pK_a = 4$, 298 K), which is unreactive towards H_2O_2 and any other organic or inorganic species (Bokare and Choi, 2011). When pH increases to neutral and alkaline values, the hexaaquo-Cr(III) ions are hydrolyzed to hydroxo-ion ($[Cr(H_2O)_5OH]^{2+}$) (Eq. 2) (Bokare and Choi, 2011). Compared to $Cr(H_2O)_6^{3+}$, $(H_2O)_5CrOH^{2+}$ ion is more reactive in anion complexation reaction (Bokare and Choi, 2011), including with HO_2^-, which is a soluble species of H_2O_2 ($pK_a = 11.65$, 298 K) (Panarin et al., 2007).

$$Cr(OH)_3 + H_2O_2 + 2OH^- \rightarrow CrO_4^{2-} + 3H_2O + 0.5H_2 \quad (1)$$

$$\left[Cr(H_2O)_6\right]^{3+} \rightarrow \left[Cr(H_2O)_5(OH)\right]^{2+} + H^+ \quad (2)$$

Although extensive researches have been performed on Cr(III) oxidation by H_2O_2, previous research mainly focused on $Cr(OH)_3$ or Cr^{3+} ions (Knoblowitz and Morrow, 1976; Rao et al., 2002), and much less is devoted to Cr(III) oxidation by H_2O_2 from naturally occurring $Cr_xFe_{1-x}(OH)_3$ precipitates and NOM-Cr(III) colloids (Pettine et al., 2008), which represent a major part of Cr cycling. While previous studies have reported that organic complexed Cr(III) and mineral forms of Cr protected Cr(III) from oxidation by Mn oxides (Tzou et al., 2002) and H_2O_2 (Luo and Chatterjee, 2010; Rock et al., 2001), the underlying kinetics and mechanism of Cr(III) oxidation from $Cr_xFe_{1-x}(OH)_3$ precipitates and NOM-Cr(III) colloids by H_2O_2 is still largely unclear, which limited our ability to thoroughly estimate the fate and transport of Cr. As aforementioned, $Cr_xFe_{1-x}(OH)_3$ precipitates and NOM-Cr(III) colloids exhibit distinct property regarding reactivity and structure from $Cr(OH)_3$. Therefore, an in-depth understanding of Cr(III) oxidation from naturally occurring Cr(III) species is crucially important to assess the efficiency of remediation strategy for Cr contamination.

The objective of this study was to fundamentally investigate the kinetics and mechanisms of Cr(III) oxidation from $Cr_xFe_{1-x}(OH)_3$ precipitates and NOM-Cr(III) colloids by H_2O_2 under oxic conditions. To this end, batch experiments were conducted to investigate the impact of H_2O_2 concentration, pH, and addition of Fe^{2+} on the rates of Cr(VI) generation. Additionally, reactive oxygen species tests as well as X-ray photoelectron spectroscopy (XPS) and X-ray absorption fine structure (XAFS) spectroscopy were performed to provide more information on the underlying mechanism of Cr(III) oxidation. Findings gained from this study advance the understanding of the long-term stability of reduced Cr(III) upon the reaction with H_2O_2 under environmentally relevant conditions.

2. Experimental section

2.1. Preparation of $Cr_xFe_{1-x}(OH)_3$ precipitates and NOM-Cr(III) colloids

$Cr_xFe_{1-x}(OH)_3$ precipitates in this study are represented by $Cr_{0.5}Fe_{0.5}(OH)_3$, which was synthesized by mixing 0.1 M $Cr(NO_3)_3{\cdot}9H_2O$ and 0.1 M $Fe(NO_3)_3{\cdot}9H_2O$ stock solution at equal molar ratio adjusted to pH 7 with 1 M NaOH in dark for 24 h. Then, the suspension was washed repeatedly by ultrapure water (resistivity >18.2 MΩ cm, Milli-Q, Millipore) to remove free ions (conductivity <200 μS/cm), dispersed by ultrasonic for 15 min, and then stored in dark at 4 °C. The resulting $Cr_{0.5}Fe_{0.5}(OH)_3$ precipitate was characterized using X-ray diffraction (XRD, Bruker D8 Advance). The XRD pattern appeared similar to that of 2-line ferrihydrite (Fig. S1, Supplementary Materials), which was in line with previous reports (Pan et al., 2017; Qian et al., 2020).

NOM-Cr(III) colloids were prepared by adding Cr(III) from 0.1 M Cr (III) stock solution to a Aldrich humic acid suspension (AHA, chosen as representative NOM; details of preparation can be found in Section S1 of Supplementary Material) to reach a final Cr(III) concentration of 38.5 μM and a AHA concentration of 40 mg C/L. The hydrodynamic diameters of NOM-Cr(III) colloids, measured by dynamic light scattering (DLS) (Zetasizer Nano, Malvern), were in the range of 150–200 nm ($n = 10$).

2.2. Batch experiments

All batch experiments were conducted in duplicate in 50 mL polypropylene bottles at 24 ± 2 °C under oxic conditions, and the bottle reactors were shielded with aluminum foil to exclude any photochemical reactions. A constant stirring speed of 450 rpm was maintained by a Teflon-coated magnetic stir bar. For oxidation of Cr(III) from $Cr_{0.5}Fe_{0.5}(OH)_3$ at pH 7, an aliquot of synthesized $Cr_{0.5}Fe_{0.5}(OH)_3$ was added into a buffer solution of 10 mM 4-(2-hydroxyethyl)-1-piperazineethanesulfonic acid (HEPES, $pK_a = 7.6$) to reach a Cr(III) concentration of 38.5 μM. For oxidation of Cr(III) from NOM-Cr(III) colloids, the resulting NOM-Cr(III) suspension with an initial Cr(III) concentration of 38.5 μM and a AHA concentration of 40 mg C/L was used throughout the experiments. The selection of 40 mg C/L AHA was to emulate the humic substances concentration typically found in subsurface environments (Herbert and Bertsch, 1995; Liao et al., 2017; Liao et al., 2019a; Page et al., 2012; Peiffer et al., 1999; Wang et al., 2016). Na_2SO_4 with concentration of 50 mM was employed as background electrolyte for all Cr(III) oxidation experiments. This concentration was selected to mimic the dominant concentration of Na^+ and SO_4^{2-} in Cr-contaminated sites (Guo et al., 2020). The Cr(III) oxidation reaction was initiated by spiking reactors of $Cr_{0.5}Fe_{0.5}(OH)_3$ precipitate and NOM-Cr(III) colloids with H_2O_2 (10–1000 μM) under oxic conditions. During the whole experiment period, the reaction vials were exposed to

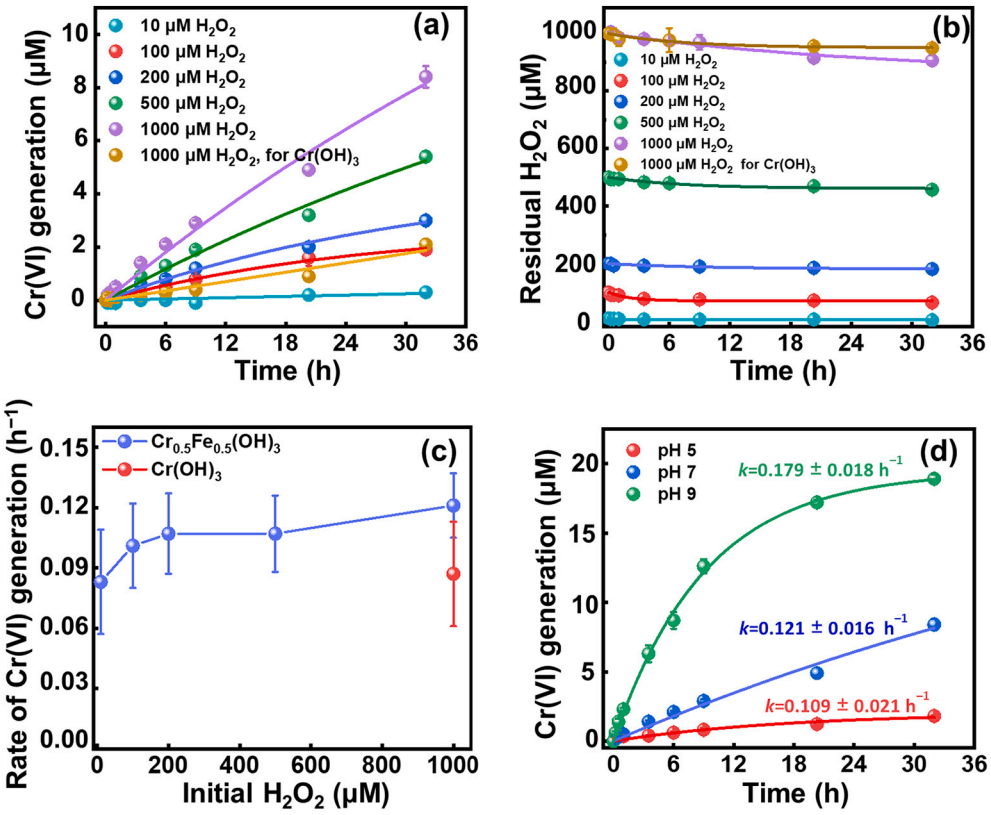

Fig. 1. (a) Cr(VI) generation from $Cr_{0.5}Fe_{0.5}(OH)_3$ precipitate by varied amount of H_2O_2 at pH 7 under oxic conditions. (b) Evolution of residual H_2O_2 concentration during the oxidation of $Cr_{0.5}Fe_{0.5}(OH)_3$ precipitate at pH 7 under oxic conditions. (c) Oxidation rates of Cr(III) from $Cr_{0.5}Fe_{0.5}(OH)_3$ precipitate as a function of initial H_2O_2 concentration at pH 7 under oxic conditions. (d) Effect of pH on Cr (VI) generation from reaction of $Cr_{0.5}Fe_{0.5}(OH)_3$ precipitate with initial 1000 μM H_2O_2 under oxic conditions. The lines in panels (a), (b), and (d) are fitted via pseudo-first-order equation of $C_t = C_{eq} \bullet (1 - e^{-kt})$ (Section S4 and Table S1), where C_t and C_{eq} are the concentration at time t and equilibrium, respectively. And k is the rate constant. In some cases, the uncertainty estimates are smaller than the size of symbols. Error bars represent the standard deviation of at least duplicate measurements.

air to allow a complete equilibrium of dissolved oxygen with atmosphere ($P_{O2} = 0.21$ bar). Control experiment with $Cr(OH)_3$ oxidation by H_2O_2 was conducted to compare the oxidation rate from $Cr_{0.5}Fe_{0.5}(OH)_3$ precipitate and NOM-Cr(III) colloids.

The effect of pH (5, 7, and 9) on Cr(III) oxidation of $Cr_{0.5}Fe_{0.5}(OH)_3$ precipitate and NOM-Cr(III) colloids was explored at a fixed H_2O_2 concentration of 1000 μM. At pH 5 and pH 9, the pH values of the suspensions were buffered with 10 mM N, N′-diethylpiperazine (DEPP, $pK_a = 4.6$) and 10 mM N-cyclohexyl-2-aminoethanesulfonic acid (CHES, $pK_a = 9.3$), respectively. All the pH buffers and their concentrations were selected due to their negligible influence on metals complexation (Li et al., 2020; Pan et al., 2017). Furthermore, the effect of Fe^{2+} on Cr (III) oxidation was investigated at Fe^{2+} concentration ranging from 30 μM to 100 μM at a fixed H_2O_2 concentration of 500 μM. To clarify the contribution of •OH radicals to Cr(III) oxidation, •OH production was analyzed using a benzoic acid probe technique following previous reports (Liao et al., 2019a; Xie et al., 2021). Briefly, 20 mM benzoic acid was added into the reaction suspension of 500 μM H_2O_2 and 100 μM Fe^{2+}, where Cr(III) was absent, to react with •OH to form a stable product of *p*-hydroxybenzoic acid (*p*-HBA). To quench the •OH radicals, 1 M ethanol was added into $Cr_{0.5}Fe_{0.5}(OH)_3$ suspension with 500 μM H_2O_2 and 100 μM Fe^{2+}. The detailed analysis of *p*-HBA is provided in Section S2 of Supplementary Materials.

2.3. Aqueous and solid phase analyses

Aqueous samples filtered through a 220 nm syringe filter (PES, Millipore) were periodically collected in order to monitor the oxidation kinetics. Aqueous Cr(VI) was determined photometrically at 540 nm, and total Cr(VI) was determined after desorption treatment in 2 mM phosphate solution for 2 h (Liao et al., 2019b). Total Cr was determined using an Agilent 7700 series inductively coupled plasma spectrometry (ICP-MS) after acidification with 6% HNO_3. The residual H_2O_2 was analyzed using modified titanium sulfonate method (Eisenberg, 1943). To minimize the interference by AHA, all samples were centrifuged (14,000 *g*) for 10 min to remove AHA and the supernatants were assayed immediately. The particle size distribution of the aqueous samples was monitored by DLS.

Solid samples were characterized by surface-sensitive XPS and XAFS to determine the oxidation state and molecular structure of Cr and Fe. Solids were collected at the end of the batch experiments by centrifugation and then freeze-dried. For cryogenic XPS measurement, all samples were first precooled in liquid nitrogen (−196 °C). The frozen sample was then transferred to the XPS analysis chamber. During the whole period, the sample temperature in the analysis chamber was monitored and maintained at −160 ± 3 °C. XPS spectra were collected using a PHI Quantera SXM scanning X-ray microprobe with an Al mono source at a 100 μm X-ray spot size. The binding energies were calibrated at 284.8 eV and the spectra were processed using MultiPak v9.8 software. Cr and Fe K-edge XANES spectra were collected in fluorescence mode on the beamline 20-BM of the Advanced Photon Source (APS) at the Argonne National Laboratory. More details of XAFS measurements can be found in Section S3 of Supplementary Materials.

3. Results and discussion

3.1. Oxidation of $Cr_{0.5}Fe_{0.5}(OH)_3$ by H_2O_2

Batch experiments show that H_2O_2 oxidized Cr(III) from $Cr_{0.5}Fe_{0.5}(OH)_3$ to Cr(VI), and Cr(VI) generation increased with increasing H_2O_2 concentration (Fig. 1a). At low H_2O_2 concentration of 10 μM, Cr(VI) generation was negligible (< 0.5 μM), which can be attributed to the faster decomposition of H_2O_2 than Cr(III) oxidation. After 32 h of reaction, Cr(VI) generation reached to 1.9 μM at 100 μM H_2O_2 and further increased to 8.4 μM when H_2O_2 concentration increased to 1000 μM. This is consistent with previous reports (Peng et al., 2019; Rao et al., 2002) showing that the oxidation rate of Cr(III) hydroxide and Cr(III) ions increased proportionately with the increase of

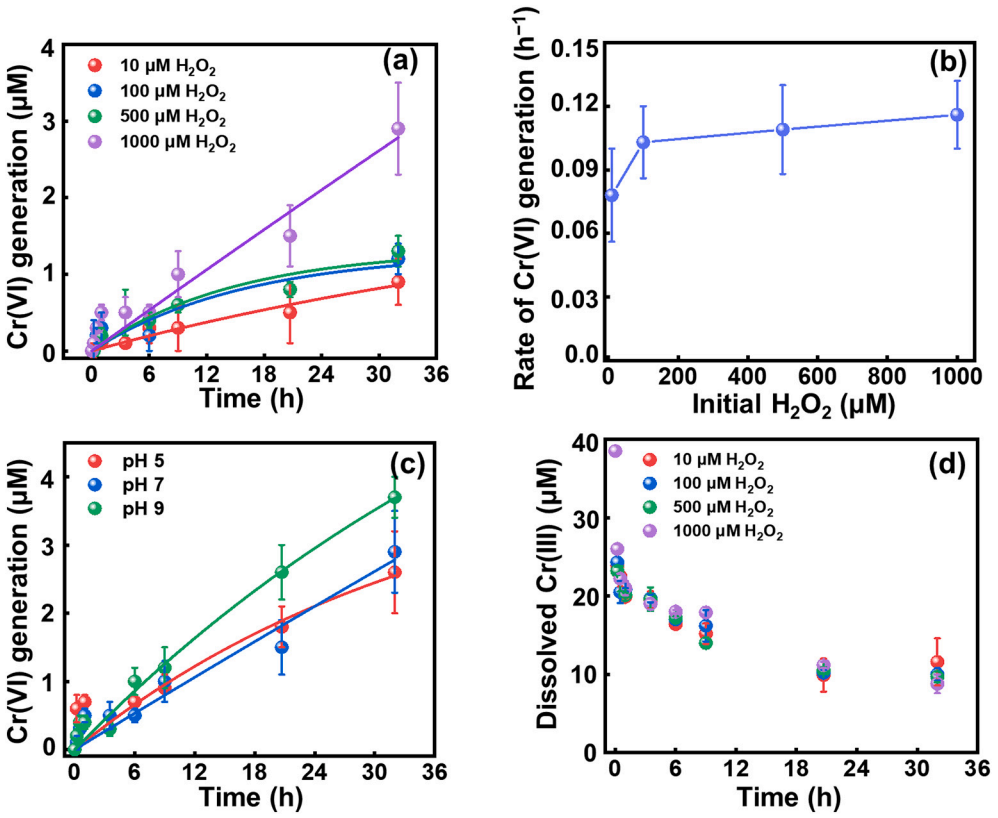

Fig. 2. (a) Generation of Cr(VI) from NOM-Cr(III) colloids upon reaction with H_2O_2 at pH 7 under oxic conditions. (b) Oxidation rates of Cr(III) from NOM-Cr(III) colloids as a function of initial H_2O_2 concentration at pH 7 under oxic conditions. (c) Effect of pH on Cr(VI) generation from reaction of NOM-Cr(III) colloids with initial 1000 μM H_2O_2 under oxic conditions. (d) Evolution of aqueous Cr(III) (through 220 nm filter) in the NOM-Cr(III) suspension upon addition of H_2O_2 at pH 7 under oxic conditions. The lines in panels (a) and (c) are fitted via pseudo-first order equation of $C_t = C_{eq} \bullet (1 - e^{-kt})$ (Section S4 and Table S1), where C_t and C_{eq} are the concentration at time t and equilibrium, respectively. And k is the rate constant. Error bars represent the standard deviation of at least duplicate measurements.

H_2O_2 concentration at pH 7. Control experiment shows that Cr(VI) generation from $Cr(OH)_3$ was only 2.1 μM after 32 h of reaction with 1000 μM H_2O_2, much lower than 8.4 μM from $Cr_{0.5}Fe_{0.5}(OH)_3$ under the same conditions. The lower generation of Cr(VI) from $Cr(OH)_3$ than from $Cr_{0.5}Fe_{0.5}(OH)_3$ was unexpected, because previous research has demonstrated that the solubility of $Cr_xFe_{1-x}(OH)_3$ plays a vital role in Cr (III) oxidation by Mn minerals (Pan et al., 2017). As aforementioned, Cr $(OH)_3$ has a higher solubility than $Cr_{0.5}Fe_{0.5}(OH)_3$, therefore, $Cr(OH)_3$ was supposed to release more Cr(III) ions into solution, favoring the formation of Cr-H_2O_2 complexes and the subsequent Cr(III) oxidation (Knoblowitz and Morrow, 1976). Therefore, the lower generation of Cr (VI) from $Cr(OH)_3$ suggests that solubility of Cr from $Cr_{0.5}Fe_{0.5}(OH)_3$ is not the determining factor controlling Cr(III) oxidation by H_2O_2. We would have proposed that the iron in $Cr_{0.5}Fe_{0.5}(OH)_3$ precipitate acted a catalyzing role that accelerated the decomposition of H_2O_2 to form reactive oxygen species (ROS) (i.e., $O_2^{\bullet-}$, •OH, or other oxidizing intermediates), thus promoting Cr(III) oxidation. However, the consumption rate of H_2O_2 in the presence of $Cr(OH)_3$ is almost the same with that in the presence of $Cr_{0.5}Fe_{0.5}(OH)_3$ (Fig. 1b), indicating that the ROS derived from H_2O_2 decomposition is not the primary oxidant responsible for Cr(III) oxidation. Therefore, Fe species seems to be the most plausible explanation for the relatively higher Cr(VI) generation from $Cr_{0.5}Fe_{0.5}(OH)_3$.

The Cr(VI) generation rates are evaluated via pseudo-first-order equation (detailed calculation is provided in Section S4 and Table S1) and plotted as a function of the initial H_2O_2 concentration (Fig. 1c). The observed rate constant (k_{obs}) of Cr(VI) generation from $Cr_{0.5}Fe_{0.5}(OH)_3$ precipitate increased slightly with increasing H_2O_2 concentration, ranging from $0.083 \pm 0.026\ h^{-1}$ at 10 μM H_2O_2 to $0.121 \pm 0.016\ h^{-1}$ at 1000 μM H_2O_2 (Fig. 1c). Furthermore, at a fixed H_2O_2 concentration of 1000 μM, k_{obs} of Cr(VI) generation from $Cr(OH)_3$ ($0.087 \pm 0.026\ h^{-1}$) is not significantly lower than that from $Cr_{0.5}Fe_{0.5}(OH)_3$. Nevertheless, a higher mean k_{obs} of the latter suggests that Fe may play a promoting role in Cr(III) oxidation by H_2O_2. More experiments were performed to decipher the role of Fe species in Cr(III) oxidation by H_2O_2, as discussed later.

Cr(III) oxidation by H_2O_2 is highly dependent on solution pH (Fig. 1d). After 32 h the generated Cr(VI) from reaction of $Cr_{0.5}Fe_{0.5}(OH)_3$ with 1000 μM H_2O_2 were 1.8 ± 0.1 μM at pH 5, 8.4 ± 0.4 μM at pH 7, and 18.9 ± 0.3 μM at pH 9. pH affects the reaction of Cr (III) with H_2O_2 in multiple ways. First, pH affects the reactivity of H_2O_2 towards Cr(III). For example, H_2O_2 acts either as an oxidant of Cr(III) ($E^0(H_2O_2/H_2O) = 1.763$ V) at pH > 8.0 (Bokare and Choi, 2011) or as a reductant of Cr(VI) ($E^0(O_2/H_2O) = 0.695$ V) under acidic conditions (Bokare and Choi, 2010; Bokare and Choi, 2011), because the reduction capability of H_2O_2 increases with decreasing pH (Bokare and Choi, 2011). Thus, increasing pH would enhance the oxidizing capability of H_2O_2 towards Cr(III) and weaken the reduction capability. Second, pH affects the hydrolysis of solubilized Cr(III) (Bokare and Choi, 2011). Increasing pH increases the hydrolysis of Cr(III) ion, as well as the oligomerization of Cr(III), thus retarding the oxidation of Cr(III) (Bokare and Choi, 2011; Rao et al., 2002). Additionally, due to the presence of iron, highly reactive Fe species may form under neutral and slightly alkaline pH conditions (Hug and Leupin, 2003). In our study, Cr(VI) generation from Cr(III) oxidation of $Cr_{0.5}Fe_{0.5}(OH)_3$ precipitate by H_2O_2 occurred at high pH, suggesting that Cr(III) oxidation by reactive oxidizing species outcompetes the effect of pH-induced oligomerization of chromium(III).

3.2. Oxidation of NOM-Cr(III) colloids

H_2O_2 also oxidized Cr(III) from NOM-Cr(III) colloids, but the oxidation extent was lower compared to $Cr_{0.5}Fe_{0.5}(OH)_3$ precipitate (Fig. 2a). As expected, the rate constant (k_{obs}) of Cr(VI) generation increased with increasing H_2O_2 concentration (Fig. 2b). The observed k_{obs} was $0.078 \pm 0.022\ h^{-1}$ at 10 μM H_2O_2, then increased slightly to $0.116 \pm 0.016\ h^{-1}$ when H_2O_2 concentration increased to 1000 μM. Compared to $Cr_{0.5}Fe_{0.5}(OH)_3$ precipitate, the effects of initial H_2O_2

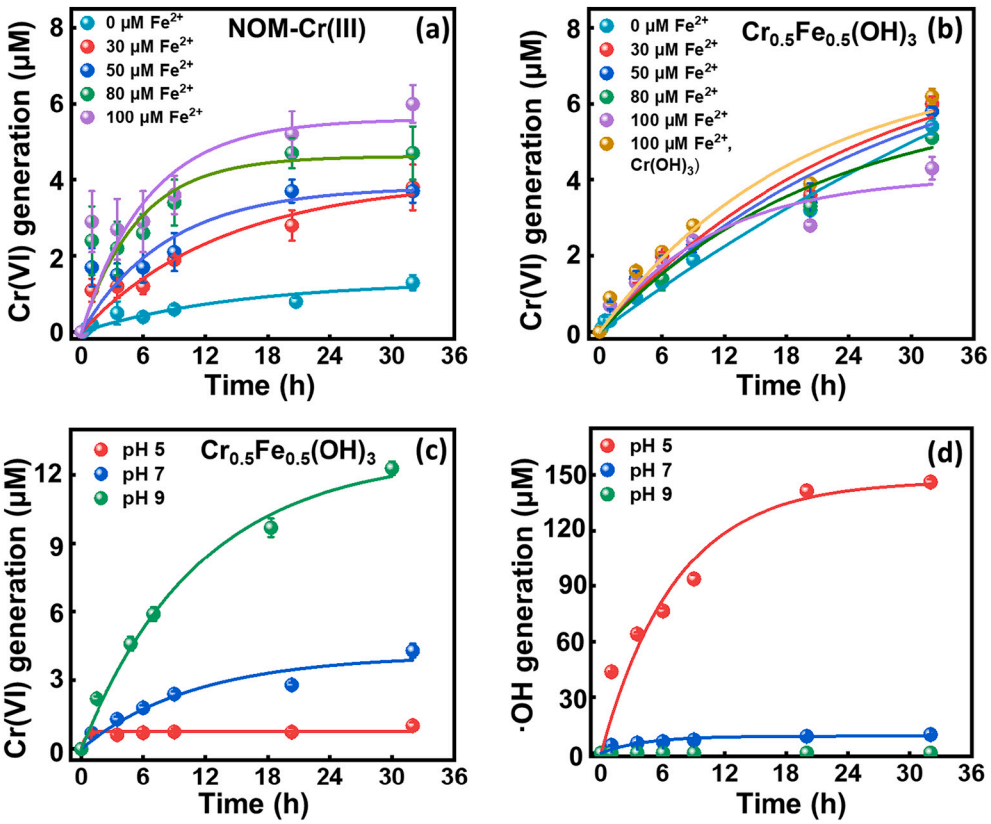

Fig. 3. Influence of Fe^{2+} on the oxidation of Cr(III) (a) from NOM-Cr(III) colloids and (b) from $Cr_{0.5}Fe_{0.5}(OH)_3$ precipitate after reaction with 500 μM H_2O_2 at pH 7 under oxic conditions. (c) Effect of pH on Cr(VI) generation from $Cr_{0.5}Fe_{0.5}(OH)_3$ precipitates after reaction of 500 μM H_2O_2 with 100 μM Fe^{2+} under oxic conditions. (d) Effect of pH on accumulative •OH production from reaction of 500 μM H_2O_2 with 100 μM Fe^{2+} concentrations under oxic conditions, where $Cr_{0.5}Fe_{0.5}(OH)_3$ precipitate and NOM-Cr(III) colloids were absent. The lines are fitted via pseudo-first order equation of $C_t = C_{eq} \bullet (1 - e^{-kt})$ (Section S4 and Table S1), where C_t and C_{eq} are the concentration at time t and equilibrium, respectively. And k is the rate constant. Error bars represent the standard deviation of at least duplicate measurements.

concentration on Cr(III) oxidation from NOM-Cr(III) colloids were smaller. According to Rock et al. (2001) and Knoblowitz and Morrow (1976), Cr(III) oxidation by H_2O_2 proceeds via forming Cr(III)-peroxide complexes first, followed by oxidation of Cr(III)-peroxide complexes to produce Cr(VI). Therefore, we would have proposed that during the oxidation of Cr(III) from NOM-Cr(III) colloids, the complexed NOM was oxidized by H_2O_2 to small organic molecules first (reaction rate constant of 1.9–2.7 × 10^4 s^{-1} (mg of C/L)$^{-1}$) (Goldstone et al., 2002; Wenk et al., 2011), exposing Cr(III) to H_2O_2, thus enabling the formation of Cr(III)-peroxide complexes for subsequent Cr(III) oxidation (reaction rate constant of 1.3–18.6 × 10^{-4} s^{-1}, calculated from Table S1). Therefore, the NOM-complexed Cr(III), to some extent, retarded oxidation of Cr(III) by H_2O_2.

Increasing pH slightly enhanced Cr(III) oxidation from NOM-Cr(III) colloids (Fig. 2c). At pH 5 and pH 7, the concentration of generated Cr (VI) was 2.6–2.9 μM after 32 h of reaction with 1000 μM H_2O_2. Further increasing the pH to 9 elevated Cr(VI) generation (i.e., 3.7 μM). The enhancement of Cr(VI) generation at alkaline pH might be related to the colloidal stabilization of NOM. The alkaline pH can inhibit the aggregation of NOM (Duval et al., 2005; Hosse and Wilkinson, 2001; Lan et al., 2022), thus enhancing their contact with water and probably promoting the complexation of Cr(III) with H_2O_2 and its subsequent oxidation. Compared to the relatively higher effect of pH on Cr(III) oxidation from $Cr_{0.5}Fe_{0.5}(OH)_3$, where reactive Fe species might form under neutral to alkaline pH, the lack of Fe in the NOM-Cr(III) colloids might explain the insignificant effect of pH on Cr(III) oxidation by H_2O_2.

Upon addition of H_2O_2, the aqueous Cr(III) concentration (through 220 nm filter) was observed to decrease immediately from initial 38.5 μM to approximately 25 μM, and further decreased continuously with reaction proceeding (Fig. 2d). The generated Cr(VI) is not adequate to account for the observed decrease in aqueous Cr(III) concentration, demonstrating that the addition of H_2O_2 decreased the colloidal stability of NOM-Cr(III) complexes, thus causing particle aggregation and precipitation. DLS results supported this proposition, showing that the hydrodynamic diameters of NOM-Cr(III) colloids increased from 150 to 200 nm to >3000 nm after addition of H_2O_2 (data not shown). During the oxidation process, the decomposition of NOM by ROS would promote the exposure of Cr(III), allowing the aggregation of positively charged Cr(III) with negatively charged moieties of NOM (Chen et al., 2022; Shin et al., 2008). Regardless of the initial H_2O_2 concentration, the decreasing trends of dissolved Cr(III) are quite similar, indicating that H_2O_2 can effectively destabilize NOM-Cr(III) colloids, potentially suppressing the transport and mobility of Cr(III) colloids.

3.3. Effect of Fe(II) on Cr(III) oxidation

Iron species affects Cr(III) oxidation from $Cr_{0.5}Fe_{0.5}(OH)_3$ precipitate and NOM-Cr(III) colloids by H_2O_2 (Fig. 3). Addition of Fe^{2+} dramatically promoted Cr(III) oxidation from NOM-Cr(III) colloids by H_2O_2 (Fig. 3a). Without Fe^{2+} addition, Cr(VI) generation from NOM-Cr(III) colloids is only 1.3 μM after 32 h of reaction with 500 μM H_2O_2, while Cr(VI) generation increased to 5.6 μM with addition of 100 μM Fe^{2+}. In contrast, Fe^{2+} exerted an insignificant influence on Cr(VI) generation from $Cr_{0.5}Fe_{0.5}(OH)_3$ precipitate (Fig. 3b). The concentrations of generated Cr(VI) were 3.9–5.6 μM after 32 h of reaction with 500 μM H_2O_2 under various Fe^{2+} concentrations. However, for $Cr(OH)_3$, addition of 100 μM Fe^{2+} dramatically increased Cr(VI) generation to ~5.8 μM (Fig. 3b), compared to ~2.1 μM from $Cr(OH)_3$ even at higher H_2O_2 concentration (1000 μM) without Fe (Fig. 1a). These observations further supported that Fe played a promoting role in Cr(III) oxidation by H_2O_2 at pH 7.

The different effects of Fe^{2+} on Cr(III) oxidation from $Cr_{0.5}Fe_{0.5}(OH)_3$ precipitate and NOM-Cr(III) colloids can be attributed to the different Fe species in their corresponding systems. In $Cr_{0.5}Fe_{0.5}(OH)_3$ suspension, the introduced Fe^{2+} was rapidly oxidized to Fe(III) by O_2 forming Fe(III) (hydr)oxides, therefore, the Fe species that is supposed to play a catalytic role in Cr(III) oxidation can only be dissolved from the newly formed Fe(III) (hydr)oxides and $Cr_{0.5}Fe_{0.5}(OH)_3$ precipitate.

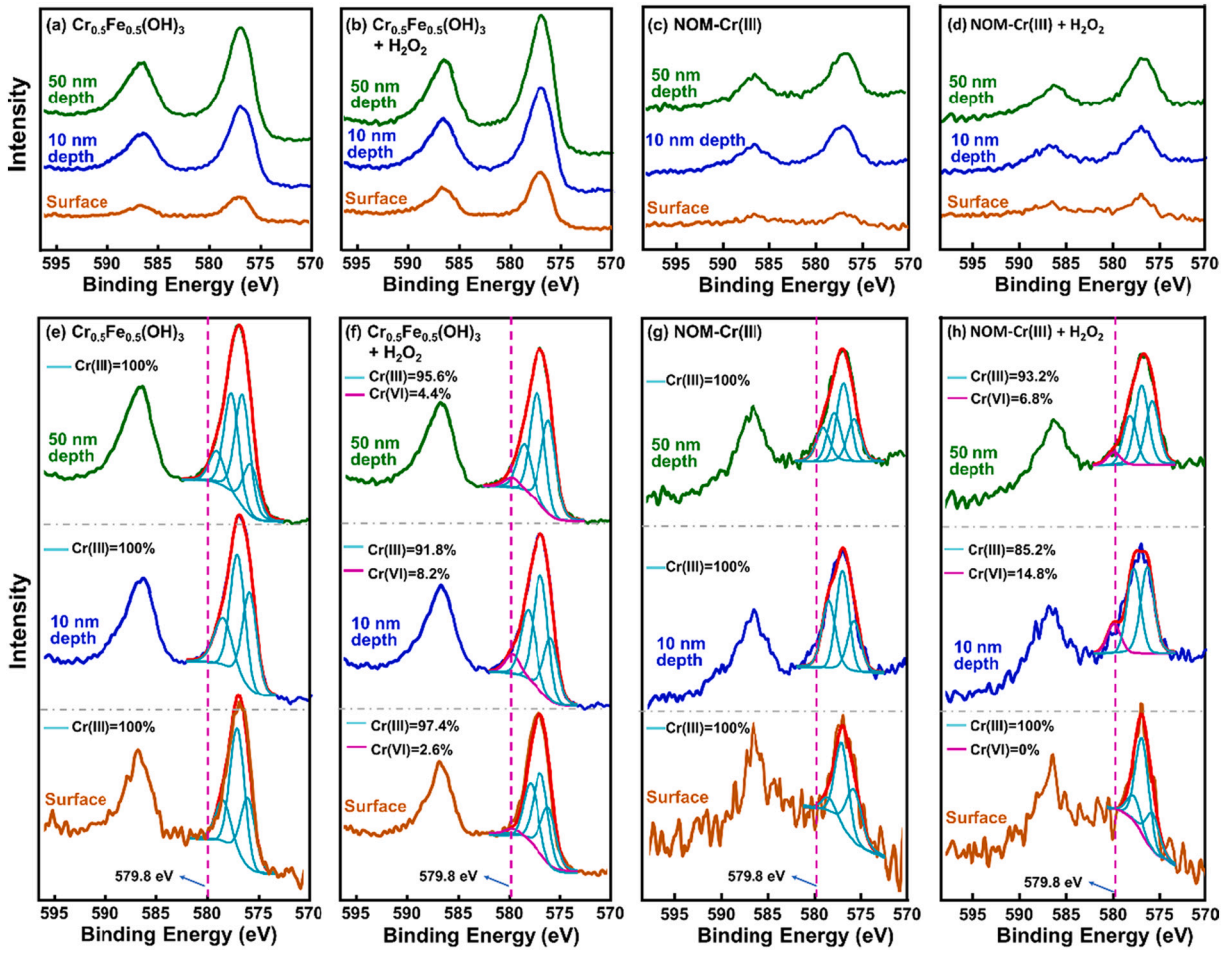

Fig. 4. Cryogenic XPS Cr 2p spectra of (a) pristine $Cr_{0.5}Fe_{0.5}(OH)_3$ precipitate and (c) pristine NOM-Cr(III) colloids prior to reaction with H_2O_2, (b) $Cr_{0.5}Fe_{0.5}(OH)_3$ precipitates and (d) NOM-Cr(III) colloids collected after 32 h of reaction with 1000 μM H_2O_2 at pH 7 under oxic conditions, respectively. The probing depths were recorded at topmost surface, 10 nm, and 50 nm depth along the sample surface. The Cr $2p_{3/2}$ spectra of pristine (e) $Cr_{0.5}Fe_{0.5}(OH)_3$ precipitate, (f) reacted $Cr_{0.5}Fe_{0.5}(OH)_3$ precipitate, (g) pristine NOM-Cr(III) colloids and (h) reacted NOM-Cr(III) colloids were fitted using a least squares procedure with the Gaussian-Lorentzian function (80% G-20% L) after subtracting a Shirley background (MultiPak v9.8). Peak fitting was performed only for the Cr $2p_{3/2}$ peak, due to the complexity of the Cr region.

Interestingly, the Cr(VI) generation is the lowest when the added Fe^{2+} concentration was highest (100 μM). It might be attributed to the fact that the addition of high Fe^{2+} concentration consumed potential ROS fast, which may decrease the oxidation efficiency of Cr(III) by H_2O_2. Furthermore, the addition of high Fe^{2+} concentration generated more iron (hydr)oxides, which might adsorb at the surface of $Cr_{0.5}Fe_{0.5}(OH)_3$ precipitate, therefore inhibiting the oxidation of Cr(III) by H_2O_2 to some extent. In contrast, in the NOM-Cr(III) system, the introduced Fe^{2+} would form NOM-Fe complexes, likely in the form of NOM-Fe colloids (Liao et al., 2017), allowing a relatively higher concentration of aqueous Fe(II) and/or Fe(III). Therefore, the catalytic effect of Fe on Cr(III) oxidation increased with increasing Fe^{2+} concentration. Altogether, the presence of iron promoted Cr(III) oxidation from $Cr_{0.5}Fe_{0.5}(OH)_3$ precipitate and NOM-Cr(III) colloids by H_2O_2 under neutral pH conditions.

Although the solubility of $Cr_{0.5}Fe_{0.5}(OH)_3$ precipitate is negligibly affected by the pH values (e.g., 5–9) (Fig. S2) (Palmer and Wittbrodt, 1991; Rai et al., 2002; Rai et al., 1987), pH significantly affects Cr(VI) generation from $Cr_{0.5}Fe_{0.5}(OH)_3$ precipitate after reaction with 500 μM H_2O_2 in the presence of 100 μM Fe^{2+} (Fig. 3c). Cr(VI) generation was 0.8 μM at pH 5, increased to 3.9 μM at pH 7, and to 12.3 μM at pH 9 towards the end of reaction. To decipher the underlying mechanism accounting for Cr(III) oxidation, •OH production was determined. The accumulative •OH production decreased dramatically with increasing pH (Fig. 3d). This confirms that Cr(VI) generation is not related to •OH production under the studied conditions. Additionally, at a fixed H_2O_2 concentration of 500 μM, the accumulative •OH production increased with increasing Fe^{2+} concentration at pH 7 (Fig. S3a), while Cr(VI) generation was almost unchanged from $Cr_{0.5}Fe_{0.5}(OH)_3$ with increasing Fe^{2+} concentration (Fig. 3b). Furthermore, the Cr(VI) generation from $Cr_{0.5}Fe_{0.5}(OH)_3$ is 3.7 μM in the presence of 1 M ethanol (Fig. S3b), slightly lower than that (5.4 μM) without addition of ethanol, further indicating that •OH is not the primary oxidant for Cr(III) oxidation. Due to the scavenge effect of NOM on oxidizing species, the effect of pH on Cr (III) oxidation from NOM-Cr(III) colloids was not as significant as from $Cr_{0.5}Fe_{0.5}(OH)_3$ (data not shown).

Despite that numerous researches (Wang et al., 2022; Xue et al., 2016; Xue et al., 2017; Ye et al., 2018) have reported the critical role of •OH in Cr(III) oxidation during Fe-mediated Fenton reactions, H_2O_2 in these studies was not added directly but was generated through Fe(II) oxidation, and decomposed to •OH rapidly. Therefore, the effect of direct oxidation of Cr(III) by H_2O_2 was significantly overlapped or even masked by •OH generation. In contrast, in this study, the amount of preexisting H_2O_2 highly exceeds the concentration of Cr(III), therefore direct oxidation of Cr(III) by H_2O_2 occurs (Bokare and Choi, 2011), in particular under neutral and alkaline conditions where oxidative effect of H_2O_2 increases while generation of •OH is significantly inhibited (Bokare and Choi, 2011). Furthermore, in the presence of iron, highly reactive Fe species are supposed to form (Hug and Leupin, 2003; Miller

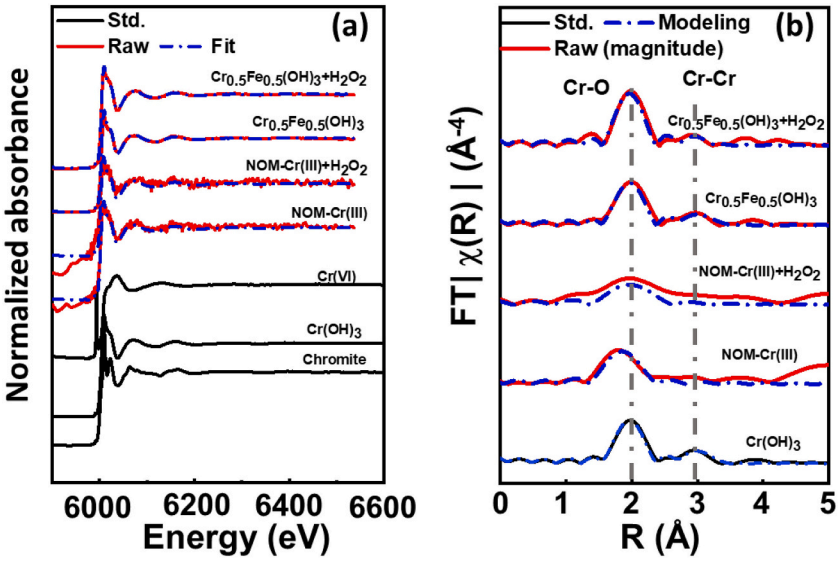

Fig. 5. (a) Cr K-edge normalized XANES spectra and (b) Cr Fourier Transforms (magnitudes) of the k^3-weighted EXAFS spectra. The red solid line, blue dot-dash line, and black solid line represent raw, fit or modeled, and standard reference compound spectra, respectively. Parameters of the EXAFS modeling are reported in Table S3. The reaction samples were collected after 32 h of reaction with H_2O_2 under oxic conditions at room temperature and pH 7. For reference, the patterns of $Cr(OH)_3$ and Cr(VI) are included in the XANES and EXAFS plots. (For interpretation of the references to colour in this figure legend, the reader is referred to the web version of this article.)

et al., 2016; Pham et al., 2020), which is more effective in Cr(III) oxidation than H_2O_2/•OH does, thus promoting Cr(III) oxidation. Consequently, the contribution of •OH to Cr(III) oxidation in this study was negligible compared to other oxidants, which might likely be highly reactive Fe species when iron is present.

Based on the above results, we speculated that the formation of highly reactive Fe species, rather than •OH, may be the main oxidant responsible for Cr(III) oxidation. This proposition is supported by previous researches conducted under comparable conditions. For example, Bi et al. (2016) proposed the formation of transient reactive Fe(III) species that drive the rapid oxidation of U(IV) to U(VI) by dissolved oxygen in the presence of FeS. Miller et al. (2016) confirmed an intermediate which is likely to be high-valent Fe species but not •OH during the oxidation of Fe(II) with H_2O_2 at circumneutral pH. Taken as a whole, we propose that the high concentration of H_2O_2 maintained the cycling of Fe between Fe(III) and Fe(II), allowing a continuous formation of highly reactive Fe species that may contribute to Cr(III) oxidation under neutral to slightly alkaline pH conditions.

3.4. Proposed mechanisms of Cr(VI) production

To further decipher the underlying mechanisms accounting for Cr (III) oxidation from $Cr_{0.5}Fe_{0.5}(OH)_3$ precipitate and NOM-Cr(III) colloids by H_2O_2, cryogenic XPS spectra in conjunction with depth profiling technique was used to identify the changes in redox state of Cr. The depth profiling technique revealed that the intensity of Cr(III) increases with increasing probing depth from the near-surface to 50 nm depth along the sample surface, indicating Cr(III) was enriched in the interior of both $Cr_{0.5}Fe_{0.5}(OH)_3$ precipitate and NOM-Cr(III) colloids (Fig. 4a–d). The elemental composition of C, O, Cr, and Fe along the probing depths was further analyzed (Table S2). For pristine $Cr_{0.5}Fe_{0.5}(OH)_3$, the Cr/Fe ratios remained largely unchanged (0.98–1.12) along the probing depths from near-surface to 50 nm depth (Table S2), which would imply that Cr and Fe are equally enriched in the $Cr_{0.5}Fe_{0.5}(OH)_3$ precipitate. After reaction with H_2O_2, the Cr/Fe ratios slightly decreased from 1.30 to 1.01 as the probing depths increased from near-surface to 10–50 nm depths. The decrease in Cr/Fe ratios along the probing depths would suggest that more Fe dissolved into aqueous phase and involved reaction with H_2O_2, perhaps forming reactive Fe species contributing to Cr(III) oxidation. The occurrence of reactive Fe species was confirmed by Bi et al. (2016), who identified a transient surface Fe(III) species by evaluating the evolution of high-spin surface Fe^{2+} species during Fe(II) oxidation. For NOM-Cr(III) colloids, low Cr/C ratio was observed at the particle near-surface (Table S2), indicating the relative enrichment of NOM at the surface of NOM-Cr(III) colloids.

Further fitting of the high-resolution Cr $2p_{3/2}$ spectra revealed that the XPS spectra of pristine $Cr_{0.5}Fe_{0.5}(OH)_3$ and NOM-Cr(III) colloids exhibit only characteristic peaks of Cr(III) at 575.9–578.5 eV (Hu et al., 2019) (Fig. 4e,g). After reaction with 1000 μM H_2O_2, a fraction of Cr(VI) at 579.8 eV (Boursiquot et al., 2002; Chai et al., 2009; Dambies et al., 2001; Hu et al., 2005) (8.2–14.8%) was present at near-surface (10 nm depth) (Fig. 4f,h). In contrast, at both the near-surface and interior (50 nm depth) of $Cr_{0.5}Fe_{0.5}(OH)_3$ precipitate and NOM-Cr(III) colloids, accumulation of Cr(VI) was lower (Fig. 4f,h), which is attributed to the dissolution of Cr(VI) from the near-surface and un-oxidation of interior Cr(III). The Cr(III) oxidation over spatial distribution suggests that the dissolution of surface Fe in $Cr_{0.5}Fe_{0.5}(OH)_3$ precipitate and the oxidation of surface NOM in the NOM-Cr(III) colloids, thus exposing Cr(III) to H_2O_2 and subsequently promoting Cr(III) oxidation.

XAFS analysis was further used to quantify the speciation and local coordination environments of Cr and Fe within $Cr_{0.5}Fe_{0.5}(OH)_3$ precipitate and NOM-Cr(III) colloids. Cr K-edge XANES spectra showed that no Cr(VI) was observed in the pristine $Cr_{0.5}Fe_{0.5}(OH)_3$ and NOM-Cr(III) samples, as evidenced by the absence of an intense pre-edge peak at ~5993 eV (Fig. 5a) (Brown et al., 2018). Even after reaction of H_2O_2, no perceptible Cr(VI) peaks can be observed (Fig. 5a). The absence of Cr(VI) peaks in XAFS may be attributed to the low amount of Cr(VI) associated with the solid samples due to the low affinity of CrO_4^{2-} to minerals. The first-shell modeling from the Cr K-edge EXAFS spectra indicated an average Cr—O distance of 1.96 Å with a coordination number of Cr ranging from 5.3 to 5.7 for pristine $Cr_{0.5}Fe_{0.5}(OH)_3$ precipitate and NOM-Cr(III) colloids, as well as H_2O_2-treated $Cr_{0.5}Fe_{0.5}(OH)_3$ precipitate (Fig. 5b and Table S3). The measured Cr—O distance was identical to that from previous reports (Gustafsson et al., 2014; Torapava et al., 2009), indicating that Cr(III) had six coordinating oxygen atoms in an octahedral geometry under the studied conditions. The coordination number for H_2O_2-treated NOM-Cr(III) decreased to 3.8 ± 1.3, which might be attributed to oligomerization of Cr(III) caused by H_2O_2 oxidation. The second shell of $Cr_{0.5}Fe_{0.5}(OH)_3$ was likely to be Cr—Cr with an average distance of 3.02 Å (Downs and Hall-Wallace, 2003), and the coordination number was 0.9–1.8. In contrast, no second shell from NOM-Cr(III) samples was observed, indicating that the Cr, O, and C atoms were not organized in a definite lattice pattern, thus confirming a poorly or non-crystalline structure in NOM-Cr(III) colloids. This NOM-mediated structure is favorable for the stability of NOM-Cr(III) colloids (Landrot et al., 2012; Li et al., 2022). However, upon reaction with

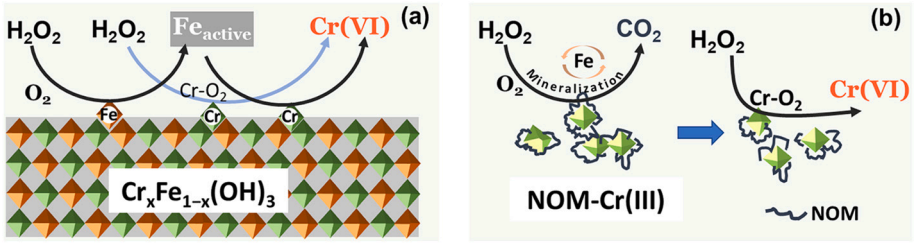

Fig. 6. Proposed mechanisms of Cr(III) oxidation from (a) $Cr_xFe_{1-x}(OH)_3$ precipitates and (b) NOM-Cr(III) colloids by H_2O_2 under oxic conditions.

H_2O_2, oxidation of complexed NOM allows the exposure of Cr(III) to H_2O_2, contributing to the formation of Cr(III)-peroxide complexes and subsequent oxidation to Cr(VI). Similarly, Fe K-edge EXAFS spectra indicated that only Fe(III) was present (section S5 and Fig. S4). Compared to ferrihydrite, the second shell from pristine $Cr_{0.5}Fe_{0.5}(OH)_3$ and H_2O_2-treated $Cr_{0.5}Fe_{0.5}(OH)_3$ has a smaller coordination number of 3.7 than that of 4.6 from ferrihydrite (Table S4), which may be favorable for the explosion of Fe to H_2O_2, thus contributing to the formation of reactive Fe species that promoted Cr(III) oxidation (Bi et al., 2016; Miller et al., 2016).

Based on the results from above series of batch experiments together with the XPS and XAFS spectra analysis, we revealed that H_2O_2 oxidizes Cr(III) from $Cr_{0.5}Fe_{0.5}(OH)_3$ precipitate and NOM-Cr(III) colloids under neutral and alkaline pH, during which iron acted a promoting role in Cr (III) oxidation. For $Cr_{0.5}Fe_{0.5}(OH)_3$ precipitate, the pathway of direct Cr (III) oxidation by H_2O_2 was slow, but the inherent Fe involved the redox reactions with H_2O_2 probably forming reactive Fe species (Hug and Leupin, 2003; Miller et al., 2016), thus accelerating Cr(III) oxidation (Fig. 6a). For NOM-Cr(III) colloids, Cr(III) oxidation by H_2O_2 proceeded via the decomposition of complexed NOM first (Goldstone et al., 2002; Katsumata et al., 2008; Wang et al., 2001), followed by the formation of Cr(III)-peroxide driving Cr(III) oxidation (Fig. 6b). Although we are unable to precisely identify the nature of reactive Fe species in our experimental settings, a large body of researches have pointed to the formation of reactive high-valent iron species during oxidation of Fe(II) with H_2O_2 and O_2 at neutral pH (Bataineh et al., 2012; Bi et al., 2016; Hug and Leupin, 2003; Keenan and Sedlak, 2008; Lee et al., 2013). Since H_2O_2 can reduce Fe(III) to Fe(II) (Gallard and De Laat, 2001), which can be subsequently oxidized back to Fe(III) by O_2 or Fe(III) hydroxides, we would have proposed that a continuous recycling between Fe(III) and Fe (II) could be maintained under the studied conditions. Considering the potential importance of Cr(III) oxidation from $Cr_xFe_{1-x}(OH)_3$ precipitates and NOM-Cr(III) colloids in engineered and natural systems, further study is required to unequivocally identify the nature and pathway of oxidant species responsible for Cr(III) oxidation by H_2O_2.

3.5. Environmental implications

Oxidation of Cr(III) to Cr(VI) poses a severe risk to ecosystem and human health. In contrast to the existing studies evaluating Cr(III) oxidation from $Cr(OH)_3$ by Mn oxides and chlorine, we provided new knowledge on the oxidation of Cr(III) from naturally occurring Cr(III) species (i.e., $Cr_xFe_{1-x}(OH)_3$ precipitates and NOM-Cr(III) colloids) by H_2O_2 under environmentally relevant conditions. For Cr(III) oxidation from $Cr_{0.5}Fe_{0.5}(OH)_3$ precipitate by 100 μM H_2O_2 at neutral pH, the rate of Cr(VI) production was observed to be $k_{obs} = 0.101 \pm 0.021$ h^{-1} (Table S1). Based on the calculated rate, it will take <2 days to produce a Cr(VI) concentration higher above the U.S. drinking water standard of 100 μg/L (1.92 μM) (Pan et al., 2019). Geochemical factors, such as pH and presence of structural Fe(III) or aqueous Fe(II), play a vital role in Cr (III) oxidation. For example, alkaline pH and the presence of iron promoted Cr(III) oxidation likely due to the formation of intermediate high active Fe species. In contrast, NOM can to some extent inhibit Cr(III) oxidation due to steric hindrance and its scavenge of oxidizing species. We acknowledge that the H_2O_2 concentrations used in this study are higher than those present in natural systems. However, high concentration of H_2O_2 is typically observed in subsurface remediation sites (Pardieck et al., 1992; Yang et al., 2019). Additionally, climate change can also elevate the level of H_2O_2 in the terrestrial and aquatic environments (Rozendal et al., 2009; Stevenson et al., 2005; Thompson, 1990; Zhang et al., 2022b). Furthermore, the in situ generated H_2O_2 might be highly concentrated at the surfaces of $Cr_xFe_{1-x}(OH)_3$ precipitates and NOM-Cr(III) colloids. Therefore, our study is important for predicting the potential risk of Cr(III) reoxidation. We certainly realize that the geochemical conditions of natural environments are much more complicated than the systems presented in this study, further investigation is needed to evaluate the rate of Cr(VI) production from $Cr_xFe_{1-x}(OH)_3$ precipitates and NOM-Cr(III) colloids upon reaction with H_2O_2 under more representative of natural conditions.

4. Conclusions

This study to our knowledge is the first report elucidating the kinetics and mechanism of Cr(III) oxidation from naturally occurring $Cr_xFe_{1-x}(OH)_3$ precipitates and NOM-Cr(III) colloids by H_2O_2 under oxic conditions. The Cr(VI) generation increases with H_2O_2 concentration, and is promoted in alkaline solution and in the presence of iron. Despite the similar k_{obs} (0.08–0.12 h^{-1}) of Cr(III) oxidation from $Cr_xFe_{1-x}(OH)_3$ precipitates and NOM-Cr(III) colloids under the studied conditions, they are appreciably larger than that from $Cr(OH)_3$. Furthermore, the presence of iron catalytically enhances the Cr oxidation from $Cr_xFe_{1-x}(OH)_3$ precipitates and NOM-Cr(III) colloids. The analysis of •OH production confirms that ROS originated from decomposition of H_2O_2 is not the principal oxidant for Cr(III) oxidation. For $Cr_xFe_{1-x}(OH)_3$ precipitates, the surface structural Fe might transform to reactive Fe species during continuous cycling of Fe(II) and Fe(III) driven by H_2O_2 at neutral to alkaline pH, which enhanced the Cr(III) oxidation. For NOM-Cr(III) colloids, the decomposition of complexed NOM by H_2O_2 enabled the formation of Cr(III)-H_2O_2 complex and the subsequent Cr(III) oxidation. The results of this study point to an underestimated pathway for Cr(VI) production by H_2O_2 from Fe(III)-Cr(III) (hydr)oxides and NOM-Cr(III) colloids in natural aquatic systems, illustrating an alternative pathway of Cr(III) re-oxidation to Cr(VI).

Declaration of Competing Interest

We (all authors) declare that we have no known competing financial interests or personal relationships that could have appeared to influence the work reported in this paper.

Data availability

Data will be made available on request.

Acknowledgments

This study was supported by the National Natural Science Foundation of China (Nos. 42177237), the Program for Guangdong Introducing

Innovative and Entrepreneurial Teams (2017ZT07Z479), the Science and Technology Planning Project of Guizhou Province (QianKeHeZhiCheng, 2022–217), and the Central Government Leading Local Science and Technology Development QianKeZhongYinDi (20214028). X-ray absorption spectroscopy analyses were performed at Beamlines 20BM of the Advanced Photon Source, Argonne National Laboratory.

Appendix A. Supplementary data

Supplementary data to this article can be found online at https://doi.org/10.1016/j.chemgeo.2022.121177.

References

Barnhart, J., 2008. Chromium chemistry and implications for environmental fate and toxicity. J. Soil Contam. 6, 561–568.
Bartlett, R., James, B., 1979. Behavior of chromium in soils: III. Oxidation. J. Environ. Qual. 8, 31–35.
Bataineh, H., Pestovsky, O., Bakac, A., 2012. pH-induced mechanistic changeover from hydroxyl radicals to iron(IV) in the Fenton reaction. Chem. Sci. 3, 1594–1599.
Bi, Y., Stylo, M., Bernier-Latmani, R., Hayes, K.F., 2016. Rapid mobilization of noncrystalline U(IV) coupled with FeS oxidation. Environ. Sci. Technol. 50, 1403–1411.
Bishop, M.E., Glasser, P., Dong, H., Arey, B., Kovarik, L., 2014. Reduction and immobilization of hexavalent chromium by microbially reduced Fe-bearing clay minerals. Geochim. Cosmochim. Acta 133, 186–203.
Bokare, A.D., Choi, W., 2010. Chromate-induced activation of hydrogen peroxide for oxidative degradation of aqueous organic pollutants. Environ. Sci. Technol. 44, 7232–7237.
Bokare, A.D., Choi, W., 2011. Advanced oxidation process based on the Cr(III)/Cr(VI) redox cycle. Environ. Sci. Technol. 45, 9332–9338.
Boman, A., Åström, M., Fröjdö, S., 2008. Sulfur dynamics in boreal acid sulfate soils rich in metastable iron sulfide—the role of artificial drainage. Chem. Geol. 255, 68–77.
Boursiquot, S., Mullet, M., Ehrhardt, J.-J., 2002. XPS study of the reaction of chromium (VI) with mackinawite (FeS). Surf. Interface Anal. 34, 293–297.
Brown, G.E., Calas, G., Waychunas, G.A., Petiau, J., 2018. Chapter 11. X-ray absorption spectroscopy and its applications in mineralogy and geochemistry. In: Frank, C.H. (Ed.), Spectroscopic Methods in Mineralogy and Geology. De Gruyter, pp. 431–512.
Chai, L., Huang, S., Yang, Z., Peng, B., Huang, Y., Chen, Y., 2009. Cr(VI) remediation by indigenous bacteria in soils contaminated by chromium-containing slag. J. Hazard. Mater. 167, 516–522.
Chang, D., Chen, T., Liu, H., Xi, Y., Qing, C., Xie, Q., Frost, R.L., 2014. A new approach to prepare ZVI and its application in removal of Cr(VI) from aqueous solution. J. Chem. Eng. 244, 264–272.
Chebeir, M., Liu, H., 2018. Oxidation of Cr(III)–Fe(III) mixed-phase hydroxides by chlorine: implications on the control of hexavalent chromium in drinking water. Environ. Sci. Technol. 52, 7663–7670.
Chen, Y., Qian, Y., Ma, J., Mao, M., Qian, L., An, D., 2022. New insights into the cooperative adsorption behavior of Cr(VI) and humic acid in water by powdered activated carbon. Sci. Total Environ. 817, 153081.
Cooper, W.J., Zika, R.G., 1983. Photochemical formation of hydrogen peroxide in surface and ground waters exposed to sunlight. Science 220, 711–712.
Cui, Y., Liu, S., Smith, K., Yu, K., Hu, H., Jiang, W., Li, Y., 2016. Characterization of corrosion scale formed on stainless steel delivery pipe for reclaimed water treatment. Water Res. 88, 816–825.
Dambies, L., Guimon, C., Yiacoumi, S., Guibal, E., 2001. Characterization of metal ion interactions with chitosan by X-ray photoelectron spectroscopy. Colloids Surf. A Physicochem. Eng. Asp. 177, 203–214.
Diem, S., Cirpka, O.A., Schirmer, M., 2013. Modeling the dynamics of oxygen consumption upon riverbank filtration by a stochastic–convective approach. J. Hydrol. 505, 352–363.
Downs, R.T., Hall-Wallace, M., 2003. The american mineralogist crystal structure database. Am. Mineral. 88, 247–250.
Duval, J.F.L., Wilkinson, K.J., van Leeuwen, H.P., Buffle, J., 2005. Humic substances are soft and permeable: evidence from their electrophoretic mobilities. Environ. Sci. Technol. 39, 6435–6445.
Eisenberg, G., 1943. Colorimetric determination of hydrogen peroxide. Ind. Eng. Chem. Anal. Ed. 15, 327–328.
Fan, X., Ding, S., Chen, M., Gao, S., Fu, Z., Gong, M., Tsang, D.C., Wang, Y., Zhang, C., 2019. Peak chromium pollution in summer and winter caused by high mobility of chromium in sediment of a eutrophic lake: in situ evidence from high spatiotemporal sampling. Environ. Sci. Technol. 53, 4755–4764.
Fandeur, D., Juillot, F., Morin, G., Olivi, L., Cognigni, A., Webb, S.M., Ambrosi, J.P., Fritsch, E., Guyot, F. Brown, Jr, G.E., 2009. XANES evidence for oxidation of Cr(III) to Cr(VI) by Mn-oxides in a lateritic regolith developed on serpentinized ultramafic rocks of New Caledonia. Environ. Sci. Technol. 43, 7384–7390.
Foustoukos, D.I., Houghton, J.L., Seyfried, W.E., Sievert, S.M., Cody, G.D., 2011. Kinetics of H_2–O_2–H_2O redox equilibria and formation of metastable H_2O_2 under low temperature hydrothermal conditions. Geochim. Cosmochim. Acta 75, 1594–1607.
Frey, M., Seidel, C., Edwards, M., Parks, J., 2005. Occurrence Survey of Boron and Hexavalent Chromium. American Water Works Association.
Gallard, H., De Laat, J., 2001. Kinetics of oxidation of chlorobenzenes and phenyl-ureas by Fe(II)/H_2O_2 and Fe(III)/H_2O_2. Evidence of reduction and oxidation reactions of intermediates by Fe(II) or Fe(III). Chemosphere 42, 405–413.
Goldstone, J.V., Pullin, M.J., Bertilsson, S., Voelker, B.M., 2002. Reactions of hydroxyl radical with humic substances: bleaching, mineralization, and production of bioavailable carbon substrates. Environ. Sci. Technol. 36, 364–372.
Guo, H., Chen, Y., Hu, H., Zhao, K., Li, H., Yan, S., Xiu, W., Coyte, R.M., Vengosh, A., 2020. High hexavalent chromium concentration in groundwater from a deep aquifer in the baiyangdian basin of the North China plain. Environ. Sci. Technol. 54, 10068–10077.
Gustafsson, J.P., Persson, I., Oromieh, A.G., van Schaik, J.W., Sjöstedt, C., Kleja, D.B., 2014. Chromium(III) complexation to natural organic matter: mechanisms and modeling. Environ. Sci. Technol. 48, 1753–1761.
Herbert, B.E., Bertsch, P.M., 1995. Characterization of dissolved and colloidal organic matter in soil solution: a review. Carbon Forms Funct. For. Soils 63–88.
Hosse, M., Wilkinson, K.J., 2001. Determination of electrophoretic mobilities and hydrodynamic radii of three humic substances as a function of pH and ionic strength. Environ. Sci. Technol. 35, 4301–4306.
Hu, J., Lo, I.M.C., Chen, G., 2004. Removal of Cr(VI) by magnetite. Water Sci. Technol. 50, 139–146.
Hu, J., Chen, G., Lo, I.M.C., 2005. Removal and recovery of Cr(VI) from wastewater by maghemite nanoparticles. Water Res. 39, 4528–4536.
Hu, Y., Xue, Q., Tang, J., Fan, X., Chen, H., 2019. New insights on Cr(VI) retention by ferrihydrite in the presence of Fe(II). Chemosphere 222, 511–516.
Hug, S.J., Leupin, O., 2003. Iron-catalyzed oxidation of arsenic(III) by oxygen and by hydrogen peroxide: pH-dependent formation of oxidants in the Fenton reaction. Environ. Sci. Technol. 37, 2734–2742.
Ivarsson, M., Broman, C., Holm, N.G., 2011. Chromite oxidation by manganese oxides in subseafloor basalts and the presence of putative fossilized microorganisms. Geochem. Trans. 12, 5.
Katsumata, H., Sada, M., Kaneco, S., Suzuki, T., Ohta, K., Yobiko, Y., 2008. Humic acid degradation in aqueous solution by the photo-Fenton process. J. Chem. Eng. 137, 225–230.
Keenan, C.R., Sedlak, D.L., 2008. Factors affecting the yield of oxidants from the reaction of nanoparticulate zero-valent iron and oxygen. Environ. Sci. Technol. 42, 1262–1267.
Knoblowitz, M., Morrow, J.I., 1976. Kinetic study of an intermediate present in the hydrogen peroxide oxidation of chromium(III) to chromium(VI). Inorg. Chem. 15, 1674–1677.
Lai, H., McNeill, L.S., 2006. Chromium redox chemistry in drinking water systems. J. Environ. Eng. 132, 842–851.
Lan, T., Wu, P., Liu, Z., Stroet, M., Liao, J., Chai, Z., Mark, A.E., Liu, N., Wang, D., 2022. Understanding the effect of pH on the solubility and aggregation extent of humic acid in solution by combining simulation and the experiment. Environ. Sci. Technol. 56, 917–927.
Landrot, G., Ginder-Vogel, M., Livi, K., Fitts, J.P., Sparks, D.L., 2012. Chromium(III) oxidation by three poorly-crystalline manganese(IV) oxides. 1. Chromium(III)-oxidizing capacity. Environ. Sci. Technol. 46, 11594–11600.
Lee, H., Lee, H.-J., Sedlak, D.L., Lee, C., 2013. pH-dependent reactivity of oxidants formed by iron and copper-catalyzed decomposition of hydrogen peroxide. Chemosphere 92, 652–658.
Li, B., Liao, P., Xie, L., Li, Q., Pan, C., Ning, Z., Liu, C., 2020. Reduced NOM triggered rapid Cr(VI) reduction and formation of NOM-Cr(III) colloids in anoxic environments. Water Res. 181, 115923.
Li, B., Liao, P., Liu, P., Wang, D., Ye, Z., Wang, J., Chen, J., Ning, Z., Jiang, Y., Liu, C., 2022. Formation, aggregation, and transport of NOM–Cr(III) colloids in aquatic environments. Environ. Sci. Nano 9, 1133–1145.
Liao, P., Li, W., Jiang, Y., Wu, J., Yuan, S., Fortner, J.D., Giammar, D.E., 2017. Formation, aggregation, and deposition dynamics of NOM-Iron colloids at anoxic–oxic interfaces. Environ. Sci. Technol. 51, 12235–12245.
Liao, P., Liang, Y., Shi, Z., 2019a. Impact of divalent cations on dark production of hydroxyl radicals from oxygenation of reduced humic acids at anoxic–oxic interfaces. ACS Earth Space Chem. 3, 484–494.
Liao, W., Ye, Z., Yuan, S., Cai, Q., Tong, M., Qian, A., Cheng, D., 2019b. Effect of coexisting Fe(III) (oxyhydr)oxides on Cr(VI) reduction by Fe(II)-bearing clay minerals. Environ. Sci. Technol. 53, 13767–13775.
Lindsay, D.R., Farley, K.J., Carbonaro, R.F., 2012. Oxidation of Cr(III) to Cr(VI) during chlorination of drinking water. J. Environ. Monit. 14, 1789–1797.
Liu, J., Chen, H., Yao, L., Wei, Z., Lou, L., Shan, Y., Endalkachew, S.D., Mallikarjuna, N., Hu, B., Zhou, X., 2016. The spatial distribution of pollutants in pipe-scale of large-diameter pipelines in a drinking water distribution system. J. Hazard. Mater. 317, 27–35.
Liu, W., Li, J., Zheng, J., Song, Y., Shi, Z., Lin, Z., Chai, L., 2020. Different pathways for Cr(III) oxidation: implications for Cr(VI) reoccurrence in reduced chromite ore processing residue. Environ. Sci. Technol. 54, 11971–11979.
Liu, X., Dong, H., Hansel, C.M., 2021. Coupled Mn(II) and Cr(III) oxidation mediated by ascomycete fungi. Environ. Sci. Technol. 55, 16236–16245.
Loyaux-Lawniczak, S., Refait, P., Ehrhardt, J.-J., Lecomte, P., Génin, J.-M.R., 2000. Trapping of Cr by formation of ferrihydrite during the reduction of chromate ions by Fe(II)−Fe(III) hydroxysalt green rusts. Environ. Sci. Technol. 34, 438–443.
Luo, Z., Chatterjee, N., 2010. Kinetics of oxidation of Cr(III)-organic complexes by H_2O_2. Chem. Speciat. Bioavailab. 22, 25–34.
McNeill, L., McLean, J., Edwards, M., Parks, J., 2012. State of the science of hexavalent chromium in drinking water. Water Res. Found. 6666, 1–35.
Miller, C.J., Rose, A.L., Waite, T.D., 2016. Importance of iron complexation for Fenton-mediated hydroxyl radical production at circumneutral pH. Front. Mar. Sci. 3, 134.

Moffett, J.W., Zika, R.G., 1987. Reaction kinetics of hydrogen peroxide with copper and iron in seawater. Environ. Sci. Technol. 21, 804–810.
Oze, C., Bird, D.K., Fendorf, S., 2007. Genesis of hexavalent chromium from natural sources in soil and groundwater. Proc. Natl. Acad. Sci. U. S. A. 104, 6544–6549.
Oze, C., Sleep, N.H., Coleman, R.G., Fendorf, S., 2016. Anoxic oxidation of chromium. Geology 44, 543–546.
Page, S.E., Sander, M., Arnold, W.A., McNeill, K., 2012. Hydroxyl radical formation upon oxidation of reduced humic acids by oxygen in the dark. Environ. Sci. Technol. 46, 1590–1597.
Palmer, C.D., Wittbrodt, P.R., 1991. Processes affecting the remediation of chromium-contaminated sites. Environ. Health Perspect. 92, 25–40.
Pan, C., Liu, H., Catalano, J.G., Qian, A., Wang, Z., Giammar, D.E., 2017. Rates of Cr(VI) generation from $Cr_xFe_{1-x}(OH)_3$ solids upon reaction with manganese oxide. Environ. Sci. Technol. 51, 12416–12423.
Pan, C., Liu, H., Catalano, J.G., Wang, Z., Qian, A., Giammar, D.E., 2019. Understanding the roles of dissolution and diffusion in $Cr(OH)_3$ oxidation by δ-MnO_2. ACS Earth Space Chem. 3, 357–365.
Panarin, E.F., Kalnin'sh, K.K., Azanova, V.V., 2007. IR spectra and structure of poly (vinylamide) complexes with hydrogen peroxide. Polym. Sci. Ser. A 49, 275–283.
Pardieck, D.L., Bouwer, E.J., Stone, A.T., 1992. Hydrogen peroxide use to increase oxidant capacity for *in situ* bioremediation of contaminated soils and aquifers: a review. J. Contam. Hydrol. 9, 221–242.
Peiffer, S., Walton-Day, K., Macalady, D.L., 1999. The interaction of natural organic matter with iron in a wetland (Tennessee Park, Colorado) receiving acid mine drainage. Aquat. Geochem. 5, 207–223.
Peiffer, S., Kappler, A., Haderlein, S.B., Schmidt, C., Byrne, J.M., Kleindienst, S., Vogt, C., Richnow, H.H., Obst, M., Angenent, L.T., Bryce, C., 2021.
A biogeochemical–hydrological framework for the role of redox-active compounds in aquatic systems. Nat. Geosci. 14, 264–272.
Peng, H., Guo, J., Li, G., Cheng, Q., Zhou, Y., Liu, Z., Tao, C., 2019. Highly efficient oxidation of chromium (III) with hydrogen peroxide in alkaline medium. Water Sci. Technol. 79, 366–374.
Pettine, M., Gennari, F., Campanella, L., Millero, F.J., 2008. The effect of organic compounds in the oxidation kinetics of Cr(III) by H_2O_2. Geochim. Cosmochim. Acta 72, 5692–5707.
Pham, P., Rashid, M., Cai, Y., Yoshinaga, M., Dionysiou, D.D., O'Shea, K., 2020. Removal of as(III) from water using the adsorptive and photocatalytic properties of humic acid-coated magnetite nanoparticles. Nanomaterials 10, 1604.
Qian, A., Pan, C., Yuan, S., Giammar, D.E., 2020. Cr(VI) formation from $Cr_xFe_{1-x}(OH)_3$ induced by Mn(II) oxidation on the surface of $Cr_xFe_{1-x}(OH)_3$. ACS Earth Space Chem. 4, 1558–1564.
Qin, J., Li, Y., Li, S., Li, H., Lin, C., 2017a. Potential effects of rainwater-borne H_2O_2 on competitive degradation of herbicides and in the presence of humic acid. Chemosphere 170, 146–152.
Qin, J., Lin, C., Cheruiyot, P., Mkpanam, S., Good-Mary Duma, N., 2017b. Potential effects of rainwater-borne hydrogen peroxide on pollutants in stagnant water environments. Chemosphere 174, 90–97.
Rai, D., Sass, B.M., Moore, D.A., 1987. Chromium(III) hydrolysis constants and solubility of chromium(III) hydroxide. Inorg. Chem. 26, 345–349.
Rai, D., Hess, N.J., Rao, L., Zhang, Z., Felmy, A.R., Moore, D.A., Clark, S.B., Lumetta, G. J., 2002. Thermodynamic model for the solubility of $Cr(OH)_{3(am)}$ in concentrated NaOH and NaOH–$NaNO_3$ solutions. J. Solut. Chem. 31, 343–367.
Ramesh Kumar, A., Riyazuddin, P., 2012. Seasonal variation of redox species and redox rotentials in shallow groundwater: a comparison of measured and calculated redox potentials. J. Hydrol. 444, 187–198.
Rao, L., Zhang, Z., Friese, J.I., Ritherdon, B., Clark, S.B., Hess, N.J., Rai, D., 2002. Oligomerization of chromium(III) and its impact on the oxidation of chromium(III) by hydrogen peroxide in alkaline solutions. J. Chem. Soc. Dalton Trans. 2, 267–274.
Rock, M.L., James, B.R., Helz, G.R., 2001. Hydrogen peroxide effects on chromium oxidation state and solubility in four diverse, chromium-enriched soils. Environ. Sci. Technol. 35, 4054–4059.
Rozendal, R.A., Leone, E., Keller, J., Rabaey, K., 2009. Efficient hydrogen peroxide generation from organic matter in a bioelectrochemical system. Electrochem. Commun. 11, 1752–1755.
Sass, B.M., Rai, D., 1987. Solubility of amorphous chromium(III)-iron(III) hydroxide solid solutions. Inorg. Chem. 26, 2228–2232.
Schroeder, D.C., Lee, G.F., 1975. Potential transformations of chromium in natural waters. Water Air Soil Pollut. 4, 355–365.
Shin, J.Y., Spinette, R.F., O'Melia, C.R., 2008. Stoichiometry of coagulation revisited. Environ. Sci. Technol. 42, 2582–2589.
Singh, B., Sherman, D.M., Gilkes, R.J., Wells, M.A., Mosselmans, J.F.W., 2002. Incorporation of Cr, Mn and Ni into goethite (α-FeOOH): mechanism from extended X-ray absorption fine structure spectroscopy. Clay Miner. 37, 639–649.
Stevenson, D., Doherty, R., Sanderson, M., Johnson, C., Collins, B., Derwent, D., 2005. Impacts of climate change and variability on tropospheric ozone and its precursors. Faraday Discuss. 130, 41–57.
Thompson, A.M., 1990. Effects of atmospheric chemical and climate change on tropospheric ozone. Ozone Sci. Eng. 12, 177–194.
Torapava, N., Radkevich, A., Davydov, D., Titov, A., Persson, I., 2009. Composition and structure of polynuclear chromium(III) hydroxo complexes. Inorg. Chem. 48, 10383–10388.
Trolard, F., Bourrie, G., Jeanroy, E., Herbillon, A.J., Martin, H., 1995. Trace metals in natural iron oxides from laterites: a study using selective kinetic extraction. Geochim. Cosmochim. Acta 59, 1285–1297.
Tzou, Y.M., Loeppert, R.H., Wang, M.K., 2002. Effect of organic complexing ligands on Cr (III) oxidation by MnO_x. Soil Sci. 167, 729–738.
Wang, G.S., Liao, C.H., Wu, F.J., 2001. Photodegradation of humic acids in the presence of hydrogen peroxide. Chemosphere 42, 379–387.
Wang, Y., Michel, F.M., Choi, Y., Eng, P.J., Levard, C., Siebner, H., Gu, B., Bargar, J.R., Brown Jr., G.E., 2016. Pb, Cu, and Zn distributions at humic acid-coated metal-oxide surfaces. Geochim. Cosmochim. Acta 188, 407–423.
Wang, T., Zhao, D., Cao, J., Zeng, Q., Li, W., Liu, B., He, D., Liu, Y., 2022. FeS-mediated mobilization and ommobilization of Cr(III) in oxic aquatic systems. Water Res. 211, 118077.
Wenk, J., von Gunten, U., Canonica, S., 2011. Effect of dissolved organic matter on the transformation of contaminants induced by excited Triplet states and the hydroxyl radical. Environ. Sci. Technol. 45, 1334–1340.
Wielinga, B., Mizuba, M.M., Hansel, C.M., Fendorf, S., 2001. Iron promoted reduction of chromate by dissimilatory iron-reducing bacteria. Environ. Sci. Technol. 35, 522–527.
Williams, A.G.B., Scherer, M.M., 2001. Kinetics of Cr(VI) reduction by carbonate green rust. Environ. Sci. Technol. 35, 3488–3494.
Xie, W., Zhang, P., Liao, W., Tong, M., Yuan, S., 2021. Ligand-enhanced electron utilization for trichloroethylene degradation by OH during sediment oxygenation. Environ. Sci. Technol. 55, 7044–7051.
Xue, Y., Jin, W., Du, H., Zheng, S., Sun, Z., Yan, W., Zhang, Y., 2016. Electrochemical Cr (III) oxidation and mobilization by in situ generated reactive oxygen species in alkaline solution. J. Electrochem. Soc. 163, H684–H689.
Xue, Y., Zheng, S., Sun, Z., Zhang, Y., Jin, W., 2017. Alkaline electrochemical advanced oxidation process for chromium oxidation at graphitized multi-walled carbon nanotubes. Chemosphere 183, 156–163.
Yang, X., Duan, Y., Wang, J., Wang, H., Liu, H., Sedlak, D.L., 2019. Impact of peroxymonocarbonate on the transformation of organic contaminants during hydrogen peroxide in situ chemical oxidation. Environ. Sci. Technol. Lett. 6, 781–786.
Ye, Y., Shan, C., Zhang, X., Liu, H., Wang, D., Lv, L., Pan, B., 2018. Water decontamination from Cr(III)–organic complexes based on pyrite/H_2O_2: performance, mechanism, and validation. Environ. Sci. Technol. 52, 10657–10664.
Zhang, D., Liu, X., Guo, D., Li, G., Qu, J., Dong, H., 2022a. Cr(VI) reduction by siderophore alone and in combination with reduced clay minerals. Environ. Sci. Technol. 56, 12315–12324.
Zhang, Y., Zhang, N., Qian, A., Yu, C., Zhang, P., Yuan, S., 2022b. Effect of C/Fe molar ratio on H_2O_2 and •OH production during oxygenation of Fe(II)-humic acid coexisting systems. Environ. Sci. Technol. 56, 13408–13418.